Eur. Phys. J. C 22, 289–301 (2001)
Digital Object Identifier (DOI) 10.1007/s100520100805

THE EUROPEAN PHYSICAL JOURNAL C

Inclusive D^* production in photon-photon collisions at next-to-leading order QCD

G. Kramer[1], H. Spiesberger[2]

[1] II. Institut für Theoretische Physik*, Universität Hamburg, Luruper Chaussee 149, 22761 Hamburg, Germany
[2] Institut für Physik, Johannes-Gutenberg-Universität, Staudinger Weg 7, 55099 Mainz, Germany

Received: 25 September 2001 /
Published online: 5 November 2001 –

Abstract. The next-to-leading order cross section for the inclusive production of charm quarks in $\gamma\gamma$ collisions is calculated as a function of the transverse momentum p_T and the rapidity y in approaches using massive or massless charm quarks. For the direct cross section we derive the massless limit from the massive theory with the result that this limit differs from the massless version with $\overline{MS}$ factorization by finite corrections. Subtracting or adding these corrections allows us to compare the two approaches on equal footing. We establish massless and massive versions with 3 and 4 initial flavours which are shown to approach the massless approximations very fast with increasing p_T. With these results we calculate the inclusive $D^{*\pm}$ cross section in $\gamma\gamma$ collisions using realistic evolved fragmentation functions with appropriate factorization scales and compare with recent data for $d\sigma/dp_T$ from three LEP collaborations after single- and double-resolved contributions have been added.

1 Introduction

Recently the three LEP collaborations, ALEPH [1], L3 [2] and OPAL [3] have presented data for inclusive $D^{*\pm}$ production in two-photon collisions at e^+e^- center-of-mass energies close to $\sqrt{S} = 189$ GeV. Besides the total cross section σ for $\gamma + \gamma \to D^* + X$ also the differential cross sections with respect to the D^* transverse momentum, $d\sigma/dp_T$, and the pseudo-rapidity, $d\sigma/d\eta$, have been measured.

In $\gamma\gamma$ collisions, where both photons are on-shell, each of the two photons can behave as either a point-like or a hadron-like (or resolved) particle. Therefore one distinguishes in such collisions three production channels called *direct* (both particles interact point-like), *single-resolved* (one γ is point-like, the other hadron-like) and *double-resolved* (both photons are hadron-like). The resolved contributions require the knowledge of parton densities in the photon, whereas the production via two direct photons is free of such non-perturbative input. The different channels mix in higher orders of perturbation theory and thus the distinction between the direct and resolved contributions becomes scale and scheme dependent: only the sum of all three contributions is a physical cross section.

* Supported by Bundesministerium für Forschung und Technologie, Bonn, Germany, under Contract 05 HT9 GA3, and by EU Fourth Framework Program *Training and Mobility of Researchers* through Network *Quantum Chromodynamics and Deep Structure of Elementary Particles* under Contract ERBFMRX–CT98–0194 (DG12 MIHT).

The transverse momentum distribution $d\sigma/dp_T$ for the inclusive production of $D^{*\pm}$ mesons is characterized by two distinct scales, the mass m of the charmed quark and the transverse momentum p_T of the D^* or charm-quark. Depending on the ratio p_T/m, two different approaches for next-to-leading order (NLO) calculations in perturbative QCD have been used for a comparison with the experimental data [1–4]. In the so-called *massless scheme*, the charm quark is considered as an active flavour in the photon [5]. In these calculations, it is assumed that four flavours $q = u$, d, s and c are present in the photon, described by corresponding distribution functions, and all quarks are taken to be massless. The charm-quark is also an in-going parton originating from the photon in the case of the resolved contributions to the cross section and it fragments into the D^* meson similarly as the produced u, d, s quarks and the gluon g. The predictions of this approach are expected to be valid in the region of large transverse momenta $p_T \gg m$. In this scheme, calculations for the small p_T region are not reliable. The cross section diverges in the limit $p_T \to 0$ and the total cross section can not be predicted. Following the usage in deep inelastic charm production [6] we shall refer to this as the *zero-mass (ZM) 4-flavour scheme* (it corresponds to the "massless charm scheme"introduced in [7] in connection with charm production in γp collisions).

The other scheme, in which cross sections for $\gamma\gamma \to D^*\ X$ have been calculated [8], is the so-called *massive charm scheme* [7]. In the massive charm scheme the number of active massless flavours in the initial state for the

resolved contribution is equal to $n_f = 3$ and the charm quark is assumed to be massive. The massive c quark appears only in the final state. In this scheme the charm mass, $m \gg \Lambda_{QCD}$, acts as a cutoff for the initial and final state collinear singularities, and sets the scale for the perturbative calculations. The cross section factorizes into a partonic hard scattering cross section multiplied by light quark and gluon densities in the case of the resolved contributions. In leading order (LO), the direct production is described by the partonic reaction $\gamma+\gamma \to c+\bar{c}$ while the resolved contributions involve the channels $\gamma + g \to c + \bar{c}$ (single resolved) and $q + \bar{q} \to c + \bar{c}$ and $g + g \to c + \bar{c}$ (double resolved), where q are the light (massless) quarks $q = u$, d, and s. This approach has the advantage that not only the various distributions, like in rapidity and/or transverse momentum, can be predicted in the full range of p_T but also the total cross section.

One might expect that the massive approach is reasonable only in those kinematical regions where the mass m and any other characteristic scale like p_T are approximately of the same magnitude and significantly larger than Λ_{QCD}. Under these circumstances the charm mass can be used to set the renormalization scale entering the quark-gluon coupling α_s as well as the factorization scale needed to evaluate the quark and gluon densities of the photon. In NLO, terms $\propto \alpha_s \ln(p_T^2/m^2)$ arise from collinear emission of the gluon by charmed quarks at large transverse momentum or from almost collinear branching of photons or gluons into $c\bar{c}$ pairs. These terms are not expected to affect the total production rates, but they might spoil the convergence of the perturbation series and cause large scale dependencies of the NLO result at $p_T \gg m$.[1] In the massive approach the prediction of differential cross sections is thus limited to a rather small range of $p_T \simeq m$. Nevertheless, predictions of this approach have been compared to data up to $p_T \simeq 10$ GeV [8].

The proper procedure for $p_T \gg m$ is to absorb potentially large logarithms into distribution and fragmentation functions where they can be resummed by virtue of the Altarelli-Parisi equations. To implement this procedure one needs a charm contribution in the photon parton distributions (PDF) and a fragmentation function (FF) for the transition $c \to D^*$ (or any other charmed meson or baryon). Logarithms $\propto \ln(M^2/m^2)$ defined with the factorization scale M are absorbed into these distribution and fragmentation functions and remaining terms $\propto \ln(p_T^2/M^2)$ are of order $O(1)$ for the appropriate choice $M \simeq p_T$. For sufficiently large p_T the cross sections calculated with this finite charm mass method including four active flavours must approach the results described earlier with the zero-mass 4-flavour scheme [5]. Since $m \neq 0$, it is reliable also for intermediate $p_T > m$, where most of the experimental data have been obtained so far, rather than only for $p_T \gg m$. We shall call this scheme with a massive charm quark, but with terms proportional to $\alpha_s \ln(M^2/m^2)$ subtracted, the *NLO 4-flavour scheme*. The scheme described above, where this subtraction is not performed and only three light active flavours are considered will be called the *NLO 3-flavour scheme*. This latter heavy quark mass approach is also often referred to as the fixed-flavour number scheme [6] in connection with heavy quark electro-production. In the following we shall not use the term "massive charm scheme" any more, since it is ambiguous. Instead we shall refer either to the NLO 3-flavour or the NLO 4-flavour approach.

The relation of these three approaches for the process $\gamma\gamma \to D^*X$ has not been investigated in detail yet. In particular, the relation between the ZM 4-flavour and the NLO 4-flavour scheme, e.g. the question, in which range of p_T values the ZM 4-flavour scheme is a good approximation to the NLO 4-flavour scheme, has not been studied so far. Also, it is of interest to know, for which p_T the NLO 3-flavour and the NLO 4-flavour scheme produce approximately the same results. So far only differential cross sections calculated in the ZM 4-flavour and in the NLO 3-flavour scheme have been compared [9]. It was found that the two approaches differ in the definitions and relative contributions of the direct and resolved terms, but essentially agree in their sum. However, in this comparison [9], the ZM 4-flavour result was modified in so far as terms containing $\alpha_s \ln(M^2/m^2)$ have been taken into account not only at order $O(\alpha_s)$, but resumming them with the Altarelli-Parisi equations in the so-called perturbative fragmentation function approach, in which initial conditions for the FF's were taken from perturbation theory [10]. This made it difficult to pin down the finite charm-mass effects present in the NLO 3-flavour scheme.

It is the purpose of this work to fill this gap and present a comparison of results obtained in the ZM and the $m \neq 0$ 4-flavour schemes. We will identify terms in the massive theory surviving in the limit $m \to 0$ which are not present in the ZM approach where the quark mass is put to zero from the beginning. These terms describe final-state interactions and can be interpreted as a perturbative fragmentation function describing the transition from massless to massive charm quarks. Only after correcting for this difference by subtracting the final-state interaction terms from the massive theory (or adding them to the massless theory) one can expect that both theories approach each other in the large-p_T limit. This way, the $m = 0$ and the $m \neq 0$ theories can be considered on the same footing and a comparison will be sensible. In addition we shall compare also to the NLO 3-flavour scheme in order to find out the difference at small and intermediate p_T. We shall concentrate in this comparison on the direct cross section for $\gamma\gamma \to D^* X$, since this is the dominant part. A similar comparison for the single-resolved and the double-resolved cross section is left to a later study. The merging of the massive fixed-order approach and the resummed massless fragmentation approach has been investigated in [11] for hadron-hadron and photon-hadron scattering. In principle one can infer from these results the corrections due to the finite charm mass for the single- and double-resolved cross sections. This work, however, as well as the calculations

[1] Similar potentially large terms $\propto \alpha_s \ln(Q^2/m^2)$, Q being the photon virtuality, appear in the calculation of charm electro-production cross sections at next-to-leading order [6].

for $\gamma\gamma$ reactions in [9], is based on the perturbative FF's [10] approach, which is too restrictive for our purpose.

The outline of our work is as follows. In Sect. 2, we shortly describe the formulae which are used to calculate the cross section for $\gamma + \gamma \to c/\bar{c} + X$ with $m \neq 0$. We derive from these cross sections the limit $m \to 0$ and compare it with the results of the zero-mass theory which can be found in the literature. This defines the necessary subtractions in the massive theory so that it approaches the massless theory in the limit of large p_T. Section 3 contains the numerical results for the comparison of the two theoretical approaches based on different choices for the scales at which finite initial and final state terms are subtracted or absorbed into non-perturbative PDF's of the photon or FF's of the charm quark. In this section we also present comparisons to the 3-flavour scheme. After adding single- and double-resolved contributions we compare the results for the $m \neq 0$ and the $m = 0$ 4-flavour schemes to recent experimental data from LEP II. Our conclusions are summarized in Sect. 5.

2 Decomposition of the LO and NLO differential cross section

2.1 Leading-order cross section

We first consider the process

$$\gamma(p_1) + \gamma(p_2) \to c(p_3) + \bar{c}(p_4) + [g(k)] \tag{1}$$

where p_i, $i = 1, 2, 3, 4$ and k denote the momenta of the two incoming photons and the outgoing c, $\bar{c}$ quarks and a possible gluon (in square brackets), which is present when we consider the NLO corrections. Below we will describe the procedure needed to obtain differential cross sections for D^* production in $\gamma\gamma$ scattering. We have the following invariants

$$\begin{aligned} &s = (p_1 + p_2)^2,\ t = T - m^2 = (p_1 - p_3)^2 - m^2, \\ &u = U - m^2 = (p_2 - p_3)^2 - m^2 \end{aligned} \tag{2}$$

and

$$s_2 = S_2 - m^2 = (p_1 + p_2 - p_3)^2 - m^2 = s + t + u\,. \tag{3}$$

It is customary to define the dimensionless variables

$$v = 1 + \frac{t}{s},\ w = -\frac{u}{s+t} \tag{4}$$

so that

$$t = -s(1-v),\ u = -svw,\ s_2 = sv(1-w)\,. \tag{5}$$

The leading-order cross section is

$$\begin{aligned} \frac{d\sigma_{\rm LO}}{dvdw} = c(s)\delta(1-w)\Bigg(&\frac{t}{u} + \frac{u}{t} + 4\frac{sm^2}{tu} \\ &-4\left(\frac{sm^2}{tu}\right)^2\Bigg) \end{aligned} \tag{6}$$

where

$$c(s) = \frac{2\pi N_C \alpha^2 e_c^4}{s}\,. \tag{7}$$

N_C is the number of quark colours and e_c is the electric charge of the charm quark, $e_c = 2/3$. From (6) the finite charm mass corrections are clearly visible. In the next section we shall show numerical results explicitly.

2.2 The next-to-leading-order cross section

The NLO corrections consist of two parts, the virtual corrections to $\gamma + \gamma \to c + \bar{c}$ and the gluonic bremsstrahlung contributions $\gamma + \gamma \to c + \bar{c} + g$. These NLO corrections have been calculated by several groups [12–14, 9]. Only in [13] explicit formulae for the separate contributions due to one-loop diagrams and due to bremsstrahlung contributions are given in a form which allows us to derive the massless limit ($m \to 0$). The results in [13] are subdivided into three parts, the vertex plus self-energy cross section $d\sigma_{\rm VSE}$, the virtual box cross section $d\sigma_{\rm Box}$ and the gluon bremsstrahlung cross section $d\sigma_{\rm Br}$, so that the NLO single-inclusive differential cross section $d\sigma/dvdw$ is decomposed as follows

$$\frac{d\sigma_{\rm NLO}}{dvdw} = \frac{d\sigma_{\rm VSE}}{dvdw} + \frac{d\sigma_{\rm Box}}{dvdw} + \frac{d\sigma_{\rm Br}}{dvdw}\,. \tag{8}$$

The three parts in (8) have according to [13] the following structure:

$$\begin{aligned} \frac{d\sigma_{\rm VSE}}{dvdw} = \frac{C(s)}{4}\delta(1-w)\Bigg\{&2A_1\left(4\left[\zeta_2 - {\rm Li}_2\left(\frac{T}{m^2}\right)\right]\right. \\ &\times\left(1 + 3\frac{m^2}{t}\right) - \ln\left(\frac{-t}{m^2}\right) \\ &\times\left(8 - 6\frac{t}{T} - \frac{t^2}{T^2}\right) - 2 - \frac{t}{T}\Bigg) \\ &+A_2\ln\left(\frac{-t}{m^2}\right) + A_3\left[{\rm Li}_2\left(\frac{T}{m^2}\right) - \zeta_2\right] \\ &\left.+A_4 + (t \leftrightarrow u)\right\} \end{aligned} \tag{9}$$

and

$$\begin{aligned} \frac{d\sigma_{\rm Box}}{dvdw} = &\frac{C_F\alpha_s}{\pi}\frac{d\sigma_{\rm LO}}{dvdw}\frac{2m^2 - s}{s\beta}\{-2\ln x\ln\beta \\ &+2{\rm Li}_2(-x) - 2{\rm Li}_2(x) - 3\zeta_2\} \\ &+\frac{C(s)}{4}\delta(1-w)\Bigg\{-8B_1\frac{2m^2 - s}{s\beta}\ln x\ln\left(\frac{-t}{m^2}\right) \\ &+2\frac{B_2}{\beta}\left(\ln x\left[4\ln(1+x) - \ln x - 4\ln\left(\frac{-t}{m^2}\right)\right]\right. \\ &\left.+4{\rm Li}_2(-x) + 2\zeta_2\right) \\ &+2B_3\ln^2 x + 4\frac{B_4}{\beta}\ln x + 4B_5\ln\left(\frac{-t}{m^2}\right) \\ &+8B_6\ln\left(\frac{T}{m^2}\right) + 4B_7\zeta_2 + 4B_8 + (t \leftrightarrow u)\Bigg\}\,. \end{aligned} \tag{10}$$

In (10)

$$\beta = \sqrt{1-4m^2/s}\,,\ x = \frac{1-\beta}{1+\beta} \tag{11}$$

and in (9) and (10) $\zeta_2 = \pi^2/6$ and the normalisation

$$C(s) = c(s)\frac{C_F\alpha_s}{2\pi}\,. \tag{12}$$

The quantities A_i and B_i are functions of m^2, s, t and u. They are given in appendix B of [13] and will not be repeated here. The contributions (9) and (10) contain also infrared divergent terms proportional to ϵ^{-1} ($2\epsilon = 4-n$) in dimensional regularization with dimension n. They are omitted since they cancel against terms in the bremsstrahlung cross section. How these terms are distributed in $d\sigma_{\rm VSE}$ and $d\sigma_{\rm Box}$ can be inferred from [13].

The last term in (8) looks more complicated. According to [13] it can be written in the following form:

$$\begin{aligned}
\frac{d\sigma_{\rm Br}}{dvdw} = C(s)\Bigg\{ & \frac{svs_2}{4S_2}\left(\frac{s_2(s+u)}{4S_2}e_2 + \frac{2S_2}{s_2(s+u)}\ln\frac{S_2}{m^2}e_3\right.\\
& + \frac{4S_2}{m^2(s+u)^2}e_4 + I_5e_5 + I_8e_8 + I_9e_9 + I_{10}e_{10}\\
& \left. + I_{13}e_{13} + I_{15}e_{15} + I_{16}e_{16} + (t\leftrightarrow u)\right)\\
& + \frac{1}{(1-w)_+}\frac{1}{4S_2}\left(\tilde e_1 + \frac{2S_2}{\tilde y}\ln\frac{T+U-\tilde y}{T+U+\tilde y}\tilde e_6\right.\\
& + \frac{4S_2}{m^2}\tilde e_7 + s_2I_{11}\tilde e_{11} + s_2^2I_{12}\tilde e_{12} + s_2^2I_{14}\tilde e_{14}\\
& \left.+(t\leftrightarrow u)\right)\Bigg\} + \frac{C_F\alpha_s}{2\pi}\frac{d\sigma_{\rm LO}}{dvdw}\frac{1}{s\beta}\\
& \times\Bigg\{(2m^2-s)\left(4\ln x\ln\frac{sv}{m^2} + 2\ln x\right.\\
& \left. -2\left[{\rm Li}_2\left(\frac{-4\beta}{(1-\beta)^2}\right) + \ln^2 x\right]\right)\\
& +2s\beta\left[1-2\ln\frac{sv}{m^2}\right]\Bigg\}\,.
\end{aligned} \tag{13}$$

Here we used $\tilde y = \sqrt{(t+u)^2-4m^2s}$ and the coefficients $\tilde e_1$, e_2, e_3, e_4, e_5, $\tilde e_6$, $\tilde e_7$, e_8, e_9, e_{10}, $\tilde e_{11}$, $\tilde e_{12}$, e_{13}, $\tilde e_{14}$, e_{15} and e_{16} are again functions of the invariants s, t, u, s_2 and of m^2. I_5 to I_{16} are integrals over angles, which have been evaluated in [13] and are written down in appendix C of this reference.

The cross sections $d\sigma_{\rm VSE}$ and $d\sigma_{\rm Box}$ are proportional to $\delta(1-w)$. The bremsstrahlung cross section $d\sigma_{\rm Br}$ contains terms proportional to $\delta(1-w)$ and to $\left(\frac{1}{1-w}\right)_+$. Other contributions are finite for $w\to 1$, as long as $m\neq 0$. In the limit $m\to 0$ they give rise to additional terms proportional to $\delta(1-w)$, $\left(\frac{1}{1-w}\right)_+$, as well as terms proportional to $\left(\frac{\ln(1-w)}{1-w}\right)_+$.

A second approach where the mass of the charm quark is neglected from the beginning was worked out in [15] and later confirmed in [16]. With $m=0$, collinear singularities appear. They are regularized by dimensional regularization. In order to understand the differences of the two approaches, we have evaluated (9), (10) and (13) in the limit $m\to 0$. Special care must be exercised in order to recover all the terms proportional to $\delta(1-w)$, $\left(\frac{1}{1-w}\right)_+$ and $\left(\frac{\ln(1-w)}{1-w}\right)_+$. We write the result in a form which has been introduced in the calculation for massless quarks in [16]. This will allow us to identify the terms which come in addition to the massless theory in the $\overline{MS}$ factorization scheme [16]. The LO cross section for $m=0$ has the simple form

$$\begin{aligned}
\lim_{m\to 0}\frac{d\sigma_{\rm LO}}{dvdw} &= c(s)\delta(1-w)\tau_0(v) \quad \text{with}\\
\tau_0(v) &= \frac{v}{1-v} + \frac{1-v}{v}\,.
\end{aligned} \tag{14}$$

The decomposition of the NLO cross section in the limit $m\to 0$ has the form

$$\begin{aligned}
\lim_{m\to 0}\frac{d\sigma_{\rm NLO}}{dvdw} = & \left(c_1 + \tilde{\tilde c}_1\ln\frac{m^2}{s}\right)\delta(1-w)\\
& + \left(c_2 + \tilde{\tilde c}_2\ln\frac{m^2}{s}\right)\left(\frac{1}{1-w}\right)_+\\
& + c_3\left(\frac{\ln(1-w)}{1-w}\right)_+\\
& + c_5\ln v + c_6\ln(1-vw)\\
& + c_7\ln(1-v+vw) + c_8\ln(1-v)\\
& + c_9\ln w + c_{10}\ln(1-w) + c_{11}\\
& + \left(\tilde c_{11} + \tilde{\tilde c}_{11}\right)\ln\frac{m^2}{s}\\
& + c_{12}\frac{\ln(1-v+vw)}{1-w} + c_{13}\frac{\ln w}{1-w}\\
& + c_{14}\frac{\ln(\frac{1-v}{1-vw})}{1-w}\,.
\end{aligned} \tag{15}$$

The coefficients c_1,... c_{14}, $\tilde{\tilde c}_1$, $\tilde{\tilde c}_2$, $\tilde c_{11}$, and $\tilde{\tilde c}_{11}$ are either functions of v alone or of v and w. We obtained the following results for them:

$$\begin{aligned}
c_1 = C(s)\Bigg(& \ln^2(1-v)\left[\frac{2}{v} + \frac{1}{1-v} - 1\right]\\
& + \ln(1-v)\left[\frac{3}{1-v} - 1\right]\\
& + \ln^2 v\left[\frac{3}{1-v} + \frac{2}{v} - 3\right]\\
& + \ln v\left[-\frac{3}{2(1-v)} + \frac{3}{2v} + 2\right]\\
& + \left(4\zeta_2 - \frac{7}{2}\right)\tau_0(v)\Bigg) + \Delta c_1\,,
\end{aligned} \tag{16}$$

where

$$\Delta c_1 = C(s)\left(-2\ln^2 v - 2\ln v + 2\right)\tau_0(v)\,; \tag{17}$$

$$\tilde{\tilde{c}}_1 = C(s)\left(-2\ln v - \frac{3}{2}\right)\tau_0(v)\,; \tag{18}$$

$$c_2 = C(s)\left(2\ln v - \frac{3}{2}\right)\tau_0(v) + \Delta c_2\,, \tag{19}$$

where

$$\Delta c_2 = C(s)\left(-4\ln v - 2\right)\tau_0(v)\,; \tag{20}$$

$$\tilde{\tilde{c}}_2 = -2C(s)\tau_0(v)\,; \tag{21}$$

$$c_3 = 2C(s)\tau_0(v) + \Delta c_3\,, \tag{22}$$

where

$$\Delta c_3 = -4C(s)\tau_0(v)\,; \tag{23}$$

$$\begin{aligned} c_5 = C(s)\Bigg(&\frac{2v(1-v)}{(1-vw)^3} - \frac{2v}{(1-vw)^2} \\ &+\frac{v}{(1-v)(1-vw)} + \frac{2v(1-v)}{1-vw} \\ &-\frac{2v}{1-v+vw} - \frac{2}{v} - 4v + \frac{3}{vw} - \frac{2}{w} + \\ &\frac{2v}{w} + 2w + 4vw - \frac{2w}{1-v} + \frac{2w}{v}\Bigg) + \Delta c_5\,, \end{aligned} \tag{24}$$

where

$$\begin{aligned} \Delta c_5 = C(s)\Bigg(&\frac{2v}{1-v} + \frac{2v^2w}{1-v} + \frac{4}{w} - \frac{2v}{w} - \frac{4}{vw} \\ &+\frac{4v}{1-v+vw}\Bigg)\,; \end{aligned} \tag{25}$$

$$\begin{aligned} c_6 = 2C(s)\Bigg(&\frac{1}{v(1-v)w}\left(2v^3 - 2 - 3v^2 + 5v\right) \\ &+\frac{1}{1-v}\left(v^2w - 2v^2\right)\Bigg)\,; \end{aligned} \tag{26}$$

$$c_7 = -C(s)\left(\frac{4v}{1-v+vw} + \frac{2}{vw}\right)\,; \tag{27}$$

$$c_8 = \frac{2C(s)}{vw}\left(1 + (1-v)^2\right)\,; \tag{28}$$

$$c_9 = -\frac{2C(s)}{v(1-v)w}\left(v^3w^2 + v^2w - (1-v)\right)\,; \tag{29}$$

$$c_{10} = c_5 + \frac{C(s)}{w(1-v)}\left(4v^2w - 2v^2w^2 - 2v^2 - 2\right)\,; \tag{30}$$

$$\begin{aligned} c_{11} = C(s)\Bigg(&\frac{2v}{1-v+vw} - \frac{8v(1-v)}{(1-vw)^3} + \frac{7v}{(1-vw)^2} \\ &-\frac{v}{(1-v)(1-vw)}\left(2 - 7v + 3v^2\right) \\ &+4v - 2 + \frac{7}{v} + \frac{1}{1-v} \\ &-w\left(v - 2 + \frac{8}{v} + \frac{2}{1-v}\right) + \frac{2v}{w} - \frac{1}{w} + \frac{1}{2vw}\Bigg) \\ &+\Delta c_{11}\,, \end{aligned} \tag{31}$$

where

$$\begin{aligned} \Delta c_{11} = C(s)\Bigg(&\frac{2v}{1-v+vw} + \frac{1}{1-v} + \frac{w}{1-v} \\ &-w(1+v) + \frac{2}{w} - \frac{v}{w} - \frac{2}{vw} - 1\Bigg)\,; \end{aligned} \tag{32}$$

$$\begin{aligned} \tilde{c}_{11} = C(s)\Bigg(&-\frac{2v(1-v)}{(1-vw)^3} + \frac{2v}{(1-vw)^2} \\ &-\frac{v}{(1-v)(1-vw)} - \frac{2v(1-v)}{1-vw} \\ &-\frac{v}{1-v} + 4v + \frac{2}{v} - \frac{1}{vw} - \frac{v}{w} - 2vw \\ &+\frac{v^2w}{1-v} - \frac{2w}{v}\Bigg)\,; \end{aligned} \tag{33}$$

$$\begin{aligned} \tilde{\tilde{c}}_{11} = C(s)\Bigg(&\frac{2v}{1-v+vw} + \frac{v}{1-v} - \frac{1+(1-v)^2}{vw} \\ &+\frac{v^2w}{1-v}\Bigg)\,; \end{aligned} \tag{34}$$

$$c_{12} = -\frac{2C(s)}{v(1-v)}\left(1 + 2v(1-v)\right)\,; \tag{35}$$

$$c_{13} = 2C(s)\frac{1+v^2}{v(1-v)}\,; \tag{36}$$

$$c_{14} = 2C(s)\frac{1+(1-v)^2}{v(1-v)} \tag{37}$$

By comparing with appendix A of [16] we obtain agreement if we set in (15) the factorization scales $M_I^2 = M_F^2 = m^2$ and put $\Delta c_1 = \Delta c_2 = \Delta c_3 = \Delta c_5 = \Delta c_{11} = 0$ in the formulae above. This means, that the $m \to 0$ limit of the NLO correction as derived in [13] agrees with [16] with initial factorization scale $M_I^2 = m^2$ and final state factorization scale $M_F^2 = m^2$ and all Δc_i terms put to zero.

Denoting the ZM NLO result of [16] with $d\sigma_{\rm ZM}/dvdw$, we can write

$$\lim_{m\to 0}\frac{d\sigma_{\rm NLO}}{dvdw}=\frac{d\sigma_{\rm ZM}}{dvdw}\,(M_I=M_F=m)+\frac{d\sigma_{\rm FSI}}{dvdw} \qquad (38)$$

with

$$\frac{d\sigma_{\rm FSI}}{dvdw}=\Delta c_1\delta(1-w)+\Delta c_2\left(\frac{1}{(1-w)}\right)_+ +\Delta c_3\left(\frac{\ln(1-w)}{1-w}\right)_+ +\Delta c_5\ln v+\Delta c_{11}. \qquad (39)$$

In [16] terms containing initial and final state singularities have been subtracted using different factorization scales M_I and M_F, respectively. Therefore, a separation of terms proportional to $\ln(M_I^2/s)$ (coefficient $\tilde{c}_{11}$) and $\ln(M_F^2/s)$ (coefficient $\tilde{\tilde{c}}_{11}$) was possible. Starting from a calculation with $m\neq 0$, this separation can, of course, not be obtained – both terms appear with the logarithm $\ln(m^2/s)$. In our formulas (33, 34) we have split this sum in two terms so that they agree with $\tilde{c}_{11}$ and $\tilde{\tilde{c}}_{11}$ in [16]. In [16] the $\overline{MS}$ factorization scheme is defined with the spin averaging for the incoming photons taken to be $1/2(1-\epsilon)$ and not equal to $1/2$ as it is sometimes done. From our calculation we conclude that the zero-mass limit of the massive theory automatically yields the result for the $\overline{MS}$ scheme with n-dimensional photon spin averaging. By comparing with [16] we note that $\tilde{\tilde{c}}_1$ and $\tilde{\tilde{c}}_2$ originate from the final-state logarithmic terms. The initial-state logarithms have no factors proportional to $\delta(1-w)$ or $1/(1-w)_+$ and appear only in $\tilde{c}_{11}$, i.e. in the non-singular contribution for $w\to 1$. There are also no terms proportional to $\ln(\mu^2/s)$, where μ is the renormalization scale, since α_s is not renormalized in first order.

Our derivation shows that the massive theory for $\gamma+\gamma\to c/\bar{c}+X$ in the limit $m\to 0$ approaches the massless theory in $\overline{MS}$ factorization with scales $M_I^2=M_F^2=m^2$ only if the terms Δc_1, Δc_2,..., Δc_{11} are removed. This result is to be expected since the regularization of collinear singularities with a mass parameter m does not necessarily give identical results as with dimensional regularization and $m=0$ from the beginning. The difference is a sum of finite terms, which have first been derived by calculating the cross section for $e^+ + e^-\to c/\bar{c}+X$ in the two theories [10]. In [10] it was shown that the additional finite terms can be interpreted as a partonic fragmentation function $d_c^c(x,\mu_0)$ for the transition from massless to massive charm quarks, $c(m=0)\to c(m\neq 0)$. The massless theory with $\overline{MS}$ factorization has to be folded with $d_c^c(x,\mu_0)$ in order to obtain the cross section in the zero-mass limit of the massive theory. This partonic or perturbative FF in $O(\alpha_s)$ is

$$d_c^c(x,\mu_0)=\frac{C_F\alpha_s}{2\pi}\left[\frac{1+x^2}{1-x}\left(\ln\frac{\mu_0^2}{m^2}-2\ln(1-x)-2\right)\right]_+ . \qquad (40)$$

One can show that the extra terms $d\sigma_{\rm FSI}/dvdw$ can be recovered in the framework of the massless theory in [16] by convoluting $d_c^c(x,\mu_0=m)$ as a FF of the charm quark with the massless LO cross section[1]:

$$\frac{d\sigma_{\rm FSI}(p_T)}{dvdw}=\lim_{m\to 0}\frac{d\sigma_{\rm LO}(\hat{p}_T=p_T/x)}{dvdw}\otimes d_c^c\,(x,\mu_0=m)\ . \qquad (41)$$

This means that the Δc_i terms represent final-state interactions which survive in the massive theory even in the limit $m\to 0$. Therefore we have labeled their sum with the subscript "FSI". They are non-singular, i.e. not proportional to $\ln(m^2/s)$.

In [9] the expression (40) was used as a starting condition at the scale $\mu_0=m$ for the calculation of perturbative FF's at an arbitrary scale via the usual Altarelli-Parisi evolution equations in the massless approach. Our derivation shows that we obtain the same finite final-state interaction terms as in $e^+e^-\to c/\bar{c}\,X$. One expects that they appear in any process for which cross sections in the limit of the massive theory and the massless theory with common factorization are compared in NLO. We remark that such finite terms do not appear in connection with initial state factorization, since the distribution of quarks in the photon has identical non-singular terms for the two cases where one considers the massless limit of the massive theory and the theory with massless quarks.

The final result for the massless limit of the massive theory, as given by (15) with the coefficients written down in (16) to (37), can be used in two ways. On the one hand, we can compare the cross section of the original massive theory with the massless theory by calculating the cross section from the full formula (8) together with (9), (10) and (13) with the limit result in (15). In this way we can establish how the additional terms proportional to m^2 and possibly $m^2\ln m^2$, i.e. all terms which vanish for $m^2\to 0$, depend on the kinematic variables. In particular, we can find out, in which kinematical region, the massless limit in (15) is a good approximation to the massive theory. Compared to the massless cross section as derived in [16] the cross section in (15) includes the finite final-state interaction terms Δc_1, Δc_2,..., Δc_{11}, and is computed for the factorization scales $M_I^2=M_F^2=m^2$. On the other hand, it is clear that the massless approximation (15) is relevant only for $p_T^2\gg m^2$. In this case p_T^2 is the large scale, so that m^2 is not a good choice for the factorization scale. The appropriate choice is $M_I^2=M_F^2=\xi\left(m^2+p_T^2\right)$ with $\xi=O(1)$. Thus it makes much more sense to compare the two theories, massive and massless, for this choice of the factorization scales. Then the large logarithms $\propto\ln(s/m^2)$ are removed and absorbed in the PDF of the photon or in the FF of the D^* meson. These PDF's and FF's are in NLO usually constructed in the $\overline{MS}$ factorization scheme which we shall assume in the following. In order to establish the effect of terms proportional to m^2 in this more realistic case, we subtract the finite final-state interaction terms Δc_1, Δc_2, ..., Δc_{11} from the massive theory and change the factorization scale in the massive theory to

[1] The explicit form for this convolution and prescriptions for the rescaling of the kinematic variables v and w can be found in [15].

$M_I^2 = M_F^2 = \xi\left(m^2 + p_T^2\right)$ by additionally subtracting

$$\left(\frac{d\sigma}{dvdw}\right)_{\rm subtr} = \tilde{\tilde{c}}_1 \ln\frac{m^2}{M_F^2}\delta(1-w) + \tilde{\tilde{c}}_2 \ln\frac{m^2}{M_F^2}\frac{1}{(1-w)_+} + \tilde{c}_{11}\ln\frac{m^2}{M_I^2} + \tilde{\tilde{c}}_{11}\ln\frac{m^2}{M_F^2} \quad (42)$$

from the massive cross section above or equally from the massless cross section in (15), which then is identical to the result in [16]. Of course, the difference of the massive and the massless approximation will be the same as in the first case with m^2 as factorization scale, only the relative amount will change. It is clear that the two cross sections, massive or massless, for $M_I^2 = M_F^2 = \xi\left(m^2 + p_T^2\right)$ must be supplemented with a realistic choice for the $c \to D^*$ FF and with the additional single- and double-resolved cross sections having a charm contribution in the photon PDF. We remark that the latter approach makes sense only in the NLO 4-flavour scheme whereas the first approach with $M_I^2 = M_F^2 = m^2$ is meaningful only in the NLO 3-flavour scheme.

3 Numerical results

We start with presenting results for the p_T distribution of the cross section for

$$e^+(p_+) + e^-(p_-) \to c(p_3) + X\,. \quad (43)$$

For this, we have to fold the cross section given in the previous section with the quasi-real photon spectrum given in the Weizsäcker-Williams approximation by

$$f_\gamma(x) = \frac{\alpha}{2\pi}\left\{\frac{1+(1-x)^2}{x}\ln\frac{E^2\theta_c^2(1-x)^2 + m_e^2x^2}{m_e^2x^2} + 2(1-x)\left[\frac{m_e^2x}{E^2\theta_c^2(1-x)^2 + m_e^2x^2} - \frac{1}{x}\right]\right\}. \quad (44)$$

Here E is the e^+ (e^-) beam energy, θ_c the maximal angle under which the outgoing electrons (positrons) are tagged and $x = E_\gamma/E$ the fraction of the beam energy entering the $\gamma\gamma$ cross section. Fixing the transverse momentum p_T of the charm quark and its rapidity y, one can perform the integration over the energy fractions of the two photons $x_i = E_i/E$, $i = 1, 2$, with the result:

$$\frac{d\sigma}{dp_Tdy} = \frac{2p_T}{S}\int_{VW}^{V}\frac{dv}{v(1-v)}\int_{VW/v}^{1}\frac{dw}{w} f_\gamma\left(x_1 = \frac{VW}{vw}\right) f_\gamma\left(x_2 = \frac{1-V}{1-v}\right)\left.\frac{d\sigma}{dvdw}\right|_{s=x_1x_2S}, \quad (45)$$

where

$$V = 1 - \sqrt{\frac{p_T^2+m^2}{S}}e^{-y}\,,\ W = \frac{1}{V}\sqrt{\frac{p_T^2+m^2}{S}}e^{y}\,,\ S = 4E^2\,. \quad (46)$$

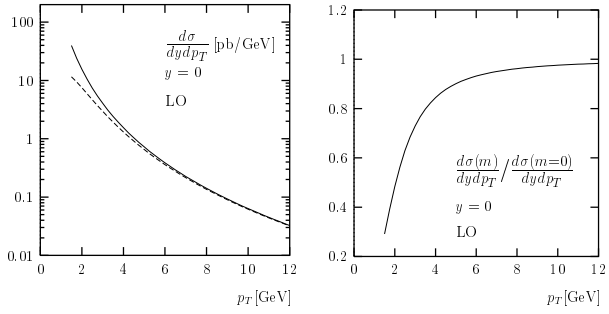

a **b**

Fig. 1. a p_T distribution $d\sigma/dydp_T$ for $e^+e^- \to \gamma\gamma \to c/\bar{c} + X \to D^{*\pm} + X$ (direct contribution, $BR(c \to D^{*\pm}) = 0.235$) at LO for $y = 0$ in the massless (*full line*) and the massive calculation (*dashed line*) with $m = 1.5$ GeV; **b** ratio of the massive and massless calculations

In the calculation with massive charm, the charm mass is kept non-zero everywhere, also in the definition of kinematic variables and phase space limits. In particular, y is the rapidity defined by $y = \frac{1}{2}\ln\frac{E_c+p_{L,c}}{E_c-p_{L,c}}$. For the comparison between various versions of the NLO cross section and their massless limits we consider the p_T distribution $d\sigma/dydp_T$ as a function of p_T for $y = 0$. Since the cross section as a function of y for fixed p_T is maximal at $y = 0$ we expect a similar behavior for the cross section $d\sigma/dp_T$ after integration over y.

In all the following comparisons the charm mass has the value $m = 1.5$ GeV. The total energy is $\sqrt{S} = 2E = 189$ GeV and the maximal angle in (44) is $\theta_c = 0.033$ in accordance with the choice in the OPAL experiment [3]. The normalization of the cross section, as given by (45) and (6) (or (14)) in the LO case is changed by multiplication with the branching ratio $BR(c \to D^*) = 0.235$. This value for BR is the average of the five experimental measurements collected and discussed in [17] ($BR = 0.235 \pm 0.007(\pm 0.007)$). A more recent value for this branching ratio based on measurements of the four LEP and the SLD experiments is $BR = 0.241 \pm 0.008$ [18]. The calculated cross sections are for the sum of c and $\bar{c}$ production. Including the branching ratio for $c \to D^*$ in the cross section will make it easier to compare the results for the cross sections without explicit FF for $c \to D^*$ with the cross sections with FF included at the end of this section. We should stress that the figures of this subsection do not include the resolved contributions so that a comparison with experimental data is not yet reasonable.

We start with the LO cross section calculated from (45) with $d\sigma/dvdw$ given in (6) and its limit for $m = 0$ in (14). The result for the two cross sections $d\sigma/dydp_T$ for $m \neq 0$ and $m = 0$, respectively, is shown in Fig. 1a. For large p_T the two cross sections approach each other. Their ratio, $d\sigma(m)/dydp_T/d\sigma(m=0)/dydp_T$, i.e. the massive over the massless cross section, as a function of p_T, is plotted in Fig. 1b. As is seen in this figure, the deviation of the massless from the massive cross section is appreciable at small p_T. The massless cross section increases strongly for

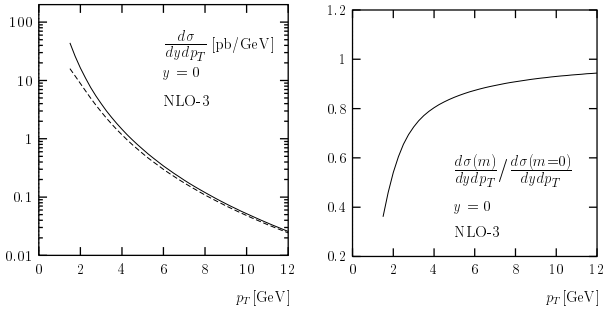

a **b**

Fig. 2. **a** p_T distribution $d\sigma/dydp_T$ in the NLO 3-flavour scheme (FSI-coefficients Δc_i added in the massless calculation, direct contribution including $BR(c \to D^{*\pm}) = 0.235$) for $y = 0$ in the massless (*full line*) and the massive calculation (*dashed line*) for $M_I = M_F = m$; **b** ratio of the massive and massless calculations

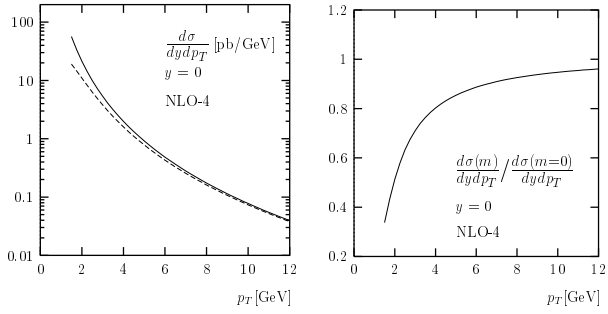

a **b**

Fig. 3. **a** p_T distribution $d\sigma/dydp_T$ in the NLO 4-flavour scheme (FSI-coefficients $\Delta c_i = 0$ in the massless calculation not resummed and subtracted in the massive calculation, direct contribution including $BR(c \to D^{*\pm}) = 0.235$) for $y = 0$ in the massless (*full line*) and the massive calculation (*dashed line*) for $M_I = M_F = \sqrt{p_T^2 + m^2}$; **b** ratio of the massive and massless calculations

$p_T \to 0$, whereas the massive cross section increases only moderately with decreasing p_T, making the ratio smaller than one. For $p_T > 5$ GeV the massive cross section differs by less than 10 % from the massless cross section. In Fig. 1b the ratio crosses the line 0.9 at $p_T = 4.9$ GeV.

In the next two figures, Fig. 2 and Fig. 3, we show the same comparison including the full NLO corrections. The value for α_s is calculated from the two-loop formula with $\Lambda_{(N_f=4)} = 328$ MeV which corresponds to $\alpha_s(m_Z) = 0.1181$ in accordance with [19]. The renormalization scale is always $\mu_R = \sqrt{p_T^2 + m^2}$ in all the results of this and the following section.

In Fig. 2a the cross section $d\sigma/dydp_T$ at $y = 0$ is shown in the NLO 3-flavour scheme. For $m \neq 0$ this is the full cross section with $d\sigma/dvdw$ in (45) calculated from (8-13). In the limit $m \to 0$ we have added the final-state-interaction coefficients Δc_i and changed the factorization scales to $M_I = M_F = m$. Only with these changes, we can expect that massive and massless cross sections approach each other for large p_T. This is indeed the case as seen in Fig. 2a,b. If we compare with the LO cross section in Fig. 1a we notice that the NLO cross section is smaller than the LO one, in particular for increasing p_T, i.e. $p_T \geq 3$ GeV. This reduction of the NLO 3-flavour cross section is due to the choice of the factorization scale $M_I = M_F = m$, which, of course, is the appropriate scale in the case of fixed three flavours. This generates negative terms in the NLO corrections which increase in absolute value with increasing p_T. These large correction terms proportional to $\ln(m^2/s)$ (see (15)) make the perturbative cross section more and more unreliable, the larger p_T is, and call for a subtraction of these terms by choosing a factorization scale determined by the large scale p_T. The subtraction terms originate predominantly from the collinear singularities in the final state and, only to a smaller extent, from the collinear singularities of the initial state (see (42) for the separation of the two parts). We remark that we used the same definition of α_s in both schemes, i.e. we took $N_f = 4$ and the same value for $\Lambda_{(N_f=4)}$ in the formula for α_s, although, for consistency with the choice of three flavours, we should have taken $N_f = 3$ and the corresponding value for $\Lambda_{(N_f=3)}$. This prescription will make it easier to compare with the results in the NLO 4-flavour scheme. The correct choice with $N_f = 3$ in α_s would have decreased the cross section shown in Fig. 2a by a few per cent. The ratio of the massive to the massless cross section in the NLO 3-flavour scheme is shown in Fig. 2b as a function of p_T. The approach towards unity with increasing p_T is slower than for the LO ratio in Fig. 1b. This is presumably caused by additional terms $\propto m^2 \ln m^2$ which are not present in LO. Now the ratio is ≥ 0.9 for $p_T \geq 7.3$ GeV, i.e. in the NLO 3-flavour scheme, larger values of p_T are required if the massless cross section should be a reasonable approximation. Towards smaller p_T the massless cross section overestimates the full massive cross section quite strongly as was already noticed in [8]. At $p_T = 2$ GeV this overestimation amounts to approximately 85 %.

The cross sections in the NLO 4-flavour scheme are plotted in Fig. 3a, again for $m \neq 0$ and $m = 0$. For $m \neq 0$ the cross section differs from the one shown in Fig. 2a by subtraction of the FSI-coefficients and by changing the factorization scales to $M_I = M_F = \sqrt{p_T^2 + m^2}$, i.e. we subtracted from the massive cross section (8-13) the terms Δc_i and the logarithms (42). The massless cross section is obtained from (15, 16-37) with $\Delta c_i = 0$, i.e. it is identical to the results of [16]. We observe that the NLO 4-flavour cross section is larger than the NLO 3-flavour cross section in Fig. 2a. About half of this difference is due to the enlarged factorization scale; the other half is due to the subtraction of the FSI-coefficients Δc_i. The increase is most effective at the larger p_T values. Without additional fragmentation effects due to the $c \to D^*$ transition the NLO 4-flavour scheme would thus lead to larger cross sections than the NLO 3-flavour scheme. The ratio of the massive and the massless cross section in the NLO 4-flavour scheme is presented in Fig. 3b. It is clear that the difference between these two cross sections is equal to

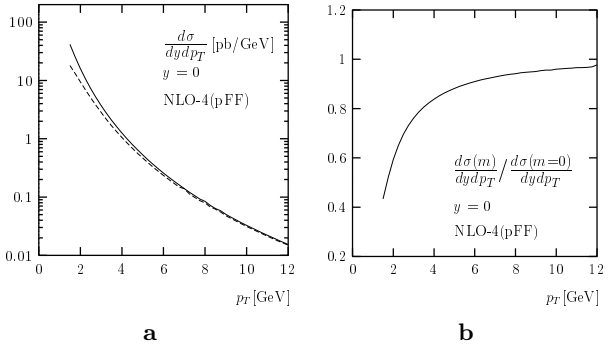

Fig. 4. As in Fig. 3, but including $c \to D^*$ fragmentation according to (40) (perturbative FF), i.e. FSI-terms resummed

the one in the NLO 3-flavour scheme shown in Fig. 2a, but the ratio changes slightly. Now, the ratio is larger than 0.9 at $p_T = 6.5$ GeV, i.e. at somewhat smaller p_T than in the NLO 3-flavour scheme (Fig. 2b).

It is clear that the results presented up to this point can not be compared to experimental data as long as no FF for the transition $c \to D^*$ is included. This deficiency is amended now for the cross section $d\sigma(y = 0)/dydp_T$ shown in Fig. 4a and Fig. 5a with two different choices of the FF. The cross sections in Fig. 4a, again for the massive and the massless version, are the cross sections in the NLO 4-flavour scheme augmented with the so called perturbative fragmentation function (pFF) [10]. The pFF is evolved via the Altarelli-Parisi equations to the appropriate scale with the initial condition at scale μ_0 equal to

$$D_c^c(x, \mu_0) = \delta(1 - x) + d_c^c(x, \mu_0) \tag{47}$$

where $d_c^c(x, \mu_0)$ is given in (40) with the choice $\mu_0 = m$ as initial scale. This prescription amounts to taking into account FSI terms not only at order $O(\alpha_s)$, but to resum them by virtue of the Altarelli-Parisi equations. The normalization of the cross sections again includes the experimental branching ratio as in the previous figures. Such a FF can be considered as a perturbative model for the real FF which we can use instead of a calculation based on non-perturbative methods. Alternatively, a FF can be extracted from experimental data for the production of D^* mesons obtained from other measurements. The latter approach will be discussed below. In Fig. 4a the perturbative FF is applied equally to the massive and massless cross sections. Through the Altarelli-Parisi evolution the terms $\propto \alpha_s(\mu) \ln(M_F/\mu_0)$ are resummed, which leads to an appreciable reduction of the cross sections at large p_T. Comparing to the cross sections in Fig. 3a the reduction amounts to a factor of more than two at $p_T = 12$ GeV. In the small-p_T region the influence of the fragmentation is largely reduced. The cross section with the pFF based on the boundary condition (47) was used in the massless approximation for a comparison with the massive NLO 3-flavour theory in [9]. Comparing with Fig. 2a we see that the two cross sections are approximately equal at $p_T \simeq 5$ GeV and the NLO 3-flavour scheme has a much larger cross section than the ZM 4-flavour scheme at $p_T = 12$ GeV in agreement with the results in Fig. 1a of [9]. The difference at larger p_T is due to the choice of scheme and the effect of the evolution of the FF in the ZM 4-flavour scheme. Of course, as in the previous figures the ZM cross section approaches the massive one for large p_T. The ratio of the two cross sections with $m \neq 0$ and $m = 0$ in the NLO 4-flavour (pFF) approach is exhibited in Fig. 4b showing that the ratio goes to one for large p_T. The ratio is larger than 0.9 for $p_T \geq 5.6$ GeV, i.e. the crossing point occurs at a smaller p_T than in the NLO 4-flavour cross section without FF (see Fig. 3b).

The approach based on perturbative fragmentation functions is, however, not sufficient to describe the fragmentation $c \to D^*$. For example, in [20] it was shown that in order to account for the inclusive production of D^* mesons in e^+e^- annihilation at various center-of-mass energies an additional non-perturbative component is needed. This means that the fragmentation of charm quarks into D^* mesons cannot be calculated in perturbation theory. A non-perturbative component, which is not known theoretically and has to be determined from other data, is always needed. Hence, it is more appropriate, to give up the perturbative component of the FF input altogether and to describe the $c \to D^*$ transition entirely by a non-perturbative FF, as it is done for the fragmentation of u, d and s quarks into light mesons. This approach has been followed in [5]. There a non-perturbative FF for $c \to D^*$ was constructed by fitting data on $e^+ + e^- \to D^* + X$ at the Z mass. For the fits two data sets from ALEPH [21] and OPAL [22] have been used. Since these two data sets are not compatible with each other, two separate fits have been performed. In the following we shall employ the results obtained from the fit to the OPAL data [5]. LEP data are best suited for such fits since they have a better accuracy as compared to lower energy data (see [5] for details). However, with LEP data there is the additional complication that one has to separate two different sources of charmed hadrons: in hadronic Z decays charmed hadrons are expected to be produced either directly through the hadronization of charmed quarks in the process $Z \to c\bar{c}$ or via weak decays of B hadrons produced in $Z \to b\bar{b}$ with approximately equal rate. With the data from [21, 22] it was possible to disentangle these two components and to construct the FF for $c \to D^*$ by determining the FF at the starting scale $\mu_0 = 2m$. At this initial value the charm-quark FF was assumed to have the Peterson form, which is particularly suitable to describe FF's that peak at large x. The Peterson FF depends only on two parameters, the normalization factor N and the shape parameter ϵ. According to [5] the fit to the OPAL data gave in NLO the values $N = 0.267$ and $\epsilon = 0.116$ resulting in a branching ratio $BR(c \to D^*) = 0.238$ at $\sqrt{S} = m_Z$ in good agreement with the average value from [17,19].

Based on the purely non-perturbative FF of [5] (OPAL set at NLO) we have calculated $d\sigma/d\eta dp_T$ at $\eta = 0$ for massive and massless quarks as a function of p_T. η is the pseudo-rapidity which was used also in the analysis of the experimental data [1–3] and we identify the pseudo-rapidity of the D^* with the rapidity of the charm quark.

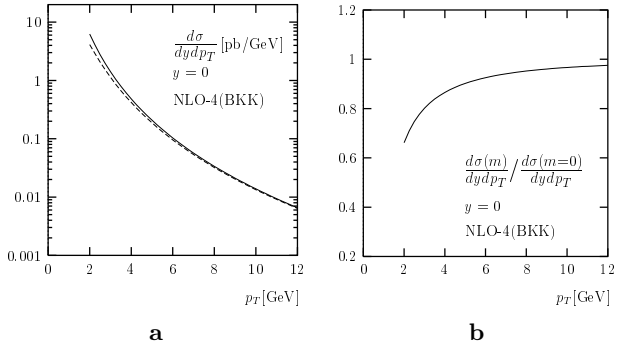

Fig. 5. As in Fig. 3, but including $c \to D^*$ fragmentation according to [5] (set OPAL NLO)

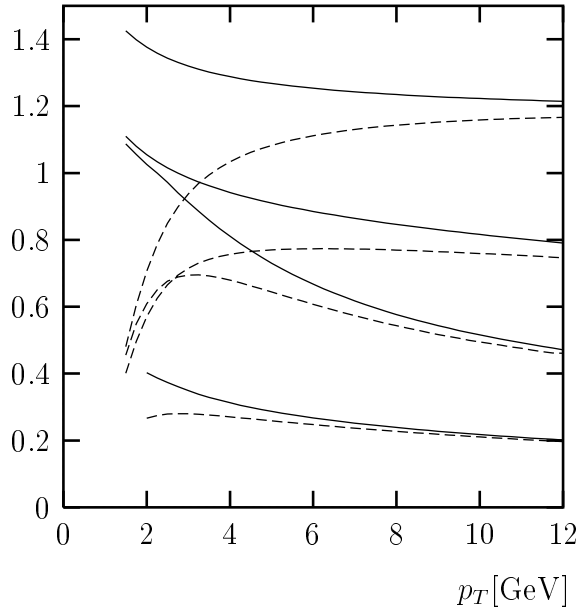

Fig. 6. p_T distributions normalized to the result of the LO massless calculation (full curve in Fig. 1a), $d\sigma/d\sigma_{\rm LO}(m=0)$ at $y = 0$. *Full lines*: massless calculations, *dashed lines*: massive calculation. From top to bottom: NLO 4-flavour scheme with $M_I = M_F = \sqrt{p_T^2 + m^2}$ (NLO-4); NLO 3-flavour scheme with $M_I = M_F = m$ (NLO-3); NLO 4-flavour scheme with $M_I = M_F = \sqrt{p_T^2 + m^2}$ including perturbative fragmentation (NLO-4(pFF)); and NLO 4-flavour scheme with non-perturbative fragmentation (NLO-4(BKK))

The resulting cross sections, denoted NLO-4(BKK), are shown for 2 GeV $< p_T <$ 12 GeV in Fig. 5a. The cross section is smaller than the one in Fig. 4a. This results essentially from the fact that the non-perturbative FF peaks at a value $x < 1$, whereas the perturbative FF is dominated by the contribution proportional to $\delta(1-x)$. For a given transverse momentum p_T of the observed D^*, smaller x in the FF probes larger $\hat{p}_T = p_T/x$ of the charm quark in the underlying hard scattering process where the cross section is smaller. The approach of the massive to the massless cross section is even faster than in the previous studies. This is seen in Fig. 5b, where the ratio is plotted. The ratio exceeds 0.9 already at $p_T = 4.7$ GeV. This stronger reduction of mass corrections is also due to the different x-dependence of the fragmentation functions since mass terms proportional to $\propto m^2/p_T^2$ decrease faster with increasing p_T than the massless cross section.

In Fig. 6 we show how the NLO results in Figs. 2, 3, 4 and 5 are related to each other. For this purpose we introduce a common normalization by dividing the results of all four, massless and massive, cross sections by the massless LO cross section (full curve in Fig. 1a). The full lines in Fig. 6 represent the massless calculations for NLO-4, NLO-3, NLO-4(pFF) and NLO-4(BKK). The dashed curves correspond to the massive cross sections. Compared to the LO massless cross section, the NLO corrections in the NLO 4-flavour scheme produce an increase of the cross section between 40 % (low p_T, massless) and 20 % (large p_T). The increase at low p_T is compensated by mass effects and at large p_T by including the pFF so that the net effect of NLO contributions in the range 3 GeV $< p_T <$ 12 GeV is a reduction between 30 % and 50 %. Most of the reduction of the NLO 3-flavour result compared to the NLO-4 curve originates from the different choice of the factorization scale. At low p_T, around $p_T \simeq 2$ GeV, the massive cross sections are approximately equal to each other. The inclusion of a fragmentation function leads to a further reduction of the cross section which is particularly strong for the case of the non-perturbative FF.

From this section we conclude that the corrections due the finite charm mass are appreciable at low p_T and are small, i.e. below 10 % for $p_T > 5$ GeV. Furthermore, the fragmentation corrections due to the evolution of the perturbative FF are also large, but now in the large-p_T region. For the non-perturbative FF there is also a reduction at smaller p_T due to the fact that in this case the hard cross section is probed at considerably larger transverse momenta of the charm quark. The approach of the massive theory towards the massless approximation is always very fast. It is strongest for the theory with a realistic, i.e. non-perturbative FF. For this case, at $p_T = 2$ GeV, the neglected mass terms lead to an overestimation of the massive result of not more than 40 %. It is also apparent, that the pure NLO 3-flavour approach, i.e. without any additional non-perturbative fragmentation corrections can give a trustworthy prediction only for rather small p_T, i.e. for $p_T < 3$ GeV. At higher p_T the effect of evolution is essential. But even at small p_T, we find a reduction by a factor 2 due to the non-perturbative FF, i.e. even at small p_T the NLO 4-flavour approach with perturbative FF does not lead to a realistic prediction for the cross section.

4 Comparison with LEPII data

Experimental data for the differential cross section $d\sigma/d\eta dp_T$ integrated over some fixed η region come from the three LEP collaborations ALEPH, L3 and OPAL. The ALEPH data [1] represent $d\sigma/dp_T$ integrated over $-1.5 < \eta < 1.5$ and are averaged over the LEPII runs with $\sqrt{S}$

in the interval 183 GeV $< \sqrt{S} <$ 189 GeV. The most recent L3 data [23] are integrated over $|\eta| < 1.4$ and averaged over 183 GeV $< \sqrt{S} <$ 209 GeV. The more recent OPAL data (second in [3]) are integrated over $|\eta| < 1.5$ with the luminosity averaged $\sqrt{S} = 193$ GeV (183 GeV $< \sqrt{S} <$ 202 GeV). We compare the three data sets of [1, 3, 23] with our calculation at $\sqrt{S} = 189$ GeV. Besides the differing $\sqrt{S}$ regions there are the slightly different regions of the η integration and possibly different anti-tagging conditions for the outgoing electrons and positrons. We disregard these differences and put the data points of all three experiments in one plot. We have checked that the different $|\eta|_{max}$ chosen by L3 on one side and ALEPH and OPAL on the other side change the cross section by at most 7 % which is much below the measurement errors of the data points. Also the different values of $\sqrt{S}$ are not expected to change the cross section by more than the corresponding experimental errors. As an example we checked that increasing $\sqrt{S}$ from 189 to 193 GeV increases $d\sigma/dp_T$ by 2 (3) % at $p_T = 2$ (12) GeV. The influence of different anti-tagging conditions could not be investigated because of insufficient information in the corresponding references.

For the comparison with the experimental data we need also the contributions of the single-resolved and double-resolved channels. They are available only in the massless approximation. Therefore we shall add the direct cross section as calculated in the previous section (in the massive and massless version) and the single-resolved and double-resolved cross sections in the massless approximation. For this we use the codes developed in [5] for the calculation of the single-resolved and double-resolved cross section for the process $\gamma\gamma \to \pi^{\pm} X$. They were also used in [24] and in the first reference of [5] for the process $\gamma p \to D^{*\pm} X$. In all cases we shall use the BKK fragmentation function as described in the previous section. We choose as factorization scales $M_I = M_F = \xi\sqrt{p_T^2 + m^2}$ with $\xi = 2$. This allows us to calculate $d\sigma/dp_T$ down to smaller p_T than previously since the starting scale of the non-perturbative FF of [5] was put equal to $2m$.

The partition of $d\sigma/d\eta dp_T$ into direct and resolved contributions, integrated over η in the region $-1.5 < \eta < 1.5$ is shown in Fig. 7. Here, DD, DR and RR denote the direct, single-resolved and double-resolved cross sections in the massless approximation and in NLO, respectively. At $p_T = 2$ GeV, these three contributions amount to approximately 38 %, 21 % and 41 % of the total sum. At $p_T = 12$ GeV the relative contributions are 71 %, 14 % and 15 %, respectively. This means that the resolved cross sections DR and RR decrease with increasing p_T much faster than the direct component DD. The separate contributions depend strongly on the factorization scales: for $M_I = M_F = \sqrt{p_T^2 + m^2}$, i.e. with $\xi = 1$, the direct contribution is larger by roughly 10 % for all p_T, the single-resolved contribution becomes steeper (with an increase of 38 % at $p_T = 2$ GeV and 3 % at $p_T = 12$ GeV), whereas the double-resolved contribution is much reduced (by 60 % at $p_T = 2$ GeV and 30 % at $p_T = 12$ GeV). We give these numbers for completeness only, although the scale dependence of the separate contributions is unphysical. The scale dependence of the physically observable cross section is weak: for the sum of all contributions these changes combine to a 13 % decrease at $p_T = 2$ GeV and a 1 % increase at $p_T = 12$ GeV. The single-resolved cross section has an appreciable component originating from the charm PDF in the photon. It is equal to 15 % at $p_T = 2$ GeV and equal to 61 % at $p_T = 12$ GeV. The double-resolved cross section is due entirely to the charm component in the photon. In Fig. 7 and the following figure the photon PDF is taken from [25], which has an explicit charm contribution.

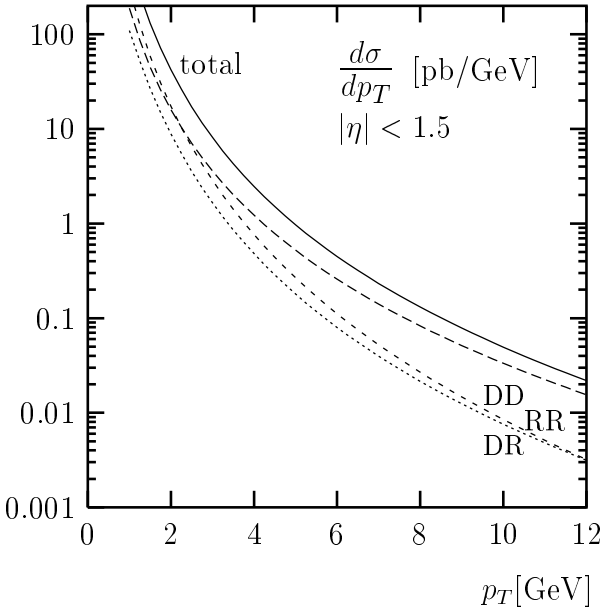

Fig. 7. Direct and resolved contributions to the p_T distribution $d\sigma/dp_T$ after integration over $|\eta| < 1.5$ at NLO with $M_I = M_F = 2\sqrt{p_T^2 + m^2}$ including BKK-fragmentation. *Upper long-dashed line*: direct, *dotted line*: single-resolved, *lower short-dashed line*: double-resolved contributions, *full line*: sum of all contributions

The sum of all three contributions, DD, DR and RR, is compared to experimental data in Fig. 8. The full curve is the cross section in the massless approximation as in Fig. 7. In the dashed curve the direct massless cross section is replaced by the direct cross section with massive quarks, i.e. NLO-4(BKK) of the previous section, except for the change of factorization scales. The resolved components are as in Fig. 7. The experimental data points shown at p_T values between 1.5 GeV and 8.5 GeV are from ALEPH [1], L3 [23] and OPAL [3]. The overall agreement between the theoretical prediction (dashed curve) and the experimental data is quite good although the data points in the medium p_T range lie slightly above the theoretical curve. Even if a finite charm mass correction for the DR and RR contributions would be included, for which we expect a reduction of the theoretical prediction by approximately 15 % at $p_T = 2$ GeV and less at higher p_T, the overall agreement for $p_T \geq 2$ GeV would hardly change. The

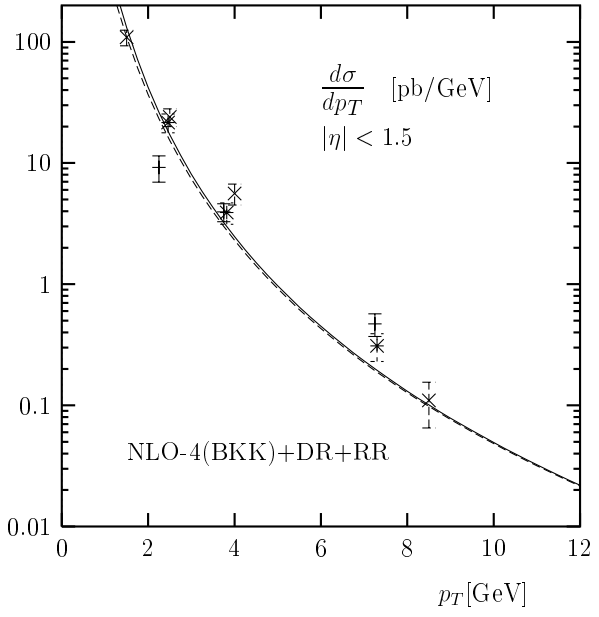

Fig. 8. p_T distribution $d\sigma/dp_T$ after integration over $|\eta| < 1.5$ in the NLO 4-flavour scheme with $M_I = M_F = 2\sqrt{p_T^2 + m^2}$ including BKK-fragmentation compared to LEP data [1,3,23]. *Full line*: massless calculation, *dashed line*: massive calculation. Single- and double-resolved contributions are included using photon PDFs of [25]

data from OPAL [3] and L3 [23] have been compared already with the predictions of the massless theory, which was obtained on the basis of the work in [5]. Compared to these results we neglected the fragmentation of the gluon $g \to D^*$. We checked that these contributions are very small at small p_T and amount to a contribution of approximately $-1\,\%$ at the largest p_T, which is negligible compared to the errors of the experimental data. This is due to the fact that the gluon enters only at NLO and that the $g \to D^*$ FF is small compared to the dominant charm FF. A similarly small effect results from a change of the charm mass. Choosing $m = 1.3$ GeV increases the cross section by $1\,\%$ in the considered p_T range between 2 GeV and 12 GeV.

5 Summary and conclusions

In this work we compared two approaches, the massive and massless schemes, for the calculation of inclusive charm production with 3 and 4 initial flavours. As a first step, the cross section $d\sigma/dp_T$ is calculated for the direct component of the $\gamma\gamma$ reaction in NLO. We found that the massless limit of the massive cross section differs from the massless theory with $\overline{MS}$ factorization by finite terms which are non-singular for $m \to 0$. A first sensible comparison of the results of the massless theory with the massive 3-flavour approach can be performed after adding these finite terms to the massless theory. The additional terms can be interpreted as the order $O(\alpha_s)$ coefficient of the perturbative fragmentation function describing final-state interactions of the transition from massless to massive charm quarks. It is clear that a resummation of these terms by using a perturbative fragmentation function is not sufficient and that one needs a non-perturbative fragmentation function (in addition to a charm distribution function in the photon). Since fragmentation and distribution functions are usually constructed in $\overline{MS}$ factorization, these terms must be subtracted also from the massive theory as soon as a fragmentation function, perturbative or non-perturbative, is taken into account. Therefore we studied the relation of this massive version with subtracted FSI terms with the massless 4-flavour approach, using different assumptions concerning the fragmentation of the c quark into D^* mesons.

It turned out that the massive versions converged rather fast to their massless limits with increasing p_T. The convergence was strongest when using non-perturbative FF fitted to e^+e^- annihilation data [5]. At low p_T, for example at $p_T = 3$ GeV, the massive cross section is reduced by approximately $20\,\%$ as compared to the massless approximation. At lower energies this reduction increases and makes the massless approximation unreliable. In addition the cross section is very much reduced by fragmentation effects, even at low p_T. This reduction increases from a factor of more than 3 at $p_T = 2$ GeV to a factor of nearly 6 at $p_T = 12$ GeV. Therefore, for reliable predictions one needs a good description of the fragmentation process. In our numerical evaluations we have taken the FF from fits to D^* production in e^+e^- annihilation at LEPI. To compare with recent measurements of the inclusive D^* cross section $d\sigma/dp_T$ in $\gamma\gamma$ reactions at LEPII we added the single- and double-resolved cross sections, which up to now are available to us only in the massless approximation. The agreement of the calculations and the data is quite good down to $p_T \simeq 1.5$ GeV even if we assume that the massless resolved contributions are reduced by a similar amount as the direct cross section. It remains to be seen whether a fit using additional experimental data to obtain a modified fragmentation function would lead to a better agreement. The fact that the data at medium p_T lie somewhat above the theoretical predictions seem to indicate that a fragmentation function which is harder than the one we used in our analysis, could be favored.

It is clear that in order to obtain results at even smaller p_T the finite charm mass corrections must be calculated also for the single- and double-resolved cross sections. Their knowledge would also be a prerequisite for the calculation of the total D^* production cross section.

Acknowledgements. We are grateful to B.A. Kniehl and M. Spira for providing us with programs for the calculation of the single- and double-resolved contributions.

References

1. ALEPH Collaboration, contributed paper # 268 to the 30th International Conference on High Energy Physics ICHEP 2000, Osaka, Japan, July 2000, ALEPH Note 2000-070.

2. M. Acciarri et al., L3 Collaboration, Phys. Lett. B467 (1999) 137
3. G. Abbiendi et al., OPAL Collaboration, Eur. Phys. J C16 (2000) 579; OPAL Collaboration, OPAL PN 453
4. A. Böhrer, hep-ph/0009121, talk at the 30th International Conference on High Energy Physics ICHEP 2000, Osaka, Japan, July 2000
5. J. Binnewies, B.A. Kniehl and G. Kramer, Phys. Rev. D 58 (1998) 014014; J. Binnewies, B.A. Kniehl and G. Kramer, Phys. Rev. D 53 (1996) 6110
6. J. Amundson, C. Schmidt, W.K. Tung and X.N. Wang, JHEP 0010 (2000) 031 and earlier papers given there
7. B.A. Kniehl, M. Krämer, G. Kramer and M. Spira, Phys. Lett. B 356 (1995) 539
8. S. Frixione, M. Krämer and E. Laenen, Nucl. Phys. B 571 (2000) 169 and earlier references given there
9. M. Cacciari, M. Greco, B.A. Kniehl, M. Krämer, G. Kramer and M. Spira, Nucl. Phys. B 466 (1996) 173
10. B. Mele and P. Nason, Nucl. Phys. B 361 (1991) 626
11. M. Cacciari, M. Greco and P. Nason, JHEP 05 (1998) 007; M. Cacciari, S. Frixione and P. Nason, JHEP 06 (2001) 0103
12. M. Drees, M. Krämer, J. Zunft and P.M. Zerwas, Phys. Lett. B 306 (1993) 371
13. B. Kamal, Z. Merebashvili and A.P. Contogouris, Phys. Rev. D 51 (1995) 4808, Erratum, Phys. Rev. D 55 (1997) 3229
14. M. Krämer and E. Laenen, Phys. Lett. B 371 (1996) 303
15. P. Aurenche, A. Douiri, R. Baier, M. Fontannaz and D. Schiff, Z. Phys. C 29 (1985) 423
16. L.E. Gordon, Phys. Rev. D 50 (1994) 6753
17. L. Gladilin, hep-ex/9912064
18. The LEP Collaborations ALEPH, DELPHI, L3, OPAL, the LEP Electroweak Working Group and the SLD Heavy Flavour and Electroweak Groups. CERN-EP/2001-021, February 28, 2001
19. D. E. Groom et al. (Particle Data Group) Eur. Phys. J. C 15 (2000) 1 (see Sect. 9)
20. P. Nason and C. Oleari, Nucl. Phys. B 565 (2000) 245
21. R. Barate et al., ALEPH Collaboration, Eur. Phys. J. C 16 (2000) 597
22. K. Ackerstaff et al., OPAL Collaboration, Eur. Phys. J. C 1 (1998) 439
23. L3 Collaboration, submitted to the International Europhysics Conference High Energy Physics 2001, Budapest, Hungary 12-18 July 2001, L3 Note 2679, July 2, 2001
24. B.A. Kniehl, G. Kramer and M. Spira, Z. Phys. C76 (1997) 689; J. Binnewies, B.A. Kniehl and G. Kramer Z. Phys. C76 (1997) 677
25. M. Glück, E. Reya and A. Vogt, Phys. Rev. D45 (1992) 3986; Phys. Rev. D46 (1992) 1973